Journal of Applied Polymer Science

Particle Clustering in Photocurable Nanocomposites: Dependence of Curing Kinetics and Viscoelastic Properties

Piotr Ziobrowski,[1] Ewa Andrzejewska,[2] Miroslaw Szybowicz,[1] Ariadna Nowicka,[1] Mariola Sadej-Bajerlein,[2] Hubert Gojzewski,[1,3] Miroslaw Drozdowski[1]

[1]Poznan University of Technology, Faculty of Technical Physics, 60-965, Poznan Poland

[2]Poznan University of Technology, Faculty of Chemical Technology, 60-965 Poznan Poland

[3]Max Planck Institute of Colloids and Interfaces, 14476 Potsdam Germany

Correspondence to: E. Andrzejewska (E-mail: ewa.andrzejewska@put.poznan.pl)

ABSTRACT: The aim of this article is to investigate the effect of nanoparticle clustering on the mobility of nanoparticles in nanocomposites, using spectroscopic methods (Brillouin and Raman). Special attention is paid to the effect of particle clustering on photocuring kinetics. The model system was poly(2-hydroxyethyl acrylate) filled with fumed nanosilica in concentration range encompassing the percolation threshold. Results obtained from Brillouin spectroscopy show substantial changes in the sound velocity and the attenuation coefficient with increasing filler content. The damping of acoustic waves reaches the maximum at the percolation threshold (~15 wt %), which is related to changes in the mechanism of acoustic wave propagation. The formation of the cocontinuous silica phase strongly affects the curing kinetics of the monomer/silica system: the polymerization rate is the highest at a silica content corresponding to the percolation threshold. These results correlate well with the results of AFM surface roughness analysis. © 2013 Wiley Periodicals, Inc. J. Appl. Polym. Sci. **2014**, *131*, 39895.

KEYWORDS: composites; kinetics; photopolymerization; viscosity and viscoelasticity; spectroscopy

Received 24 March 2013; accepted 28 August 2013

DOI: 10.1002/app.39895

INTRODUCTION

Polymer nanocomposites are intensively investigated due to their unique properties, which can be tuned by introduction of suitable nanofiller into a polymer matrix. Reinforcement of a soft polymer matrix with hard nanoparticles enhances stiffness and strength but can improve also other properties, such as thermal and barrier properties, abrasion, and fire resistance or electrical conductivity, depending on the type of nanonofiller added.[1–7]

Optimal reinforcement requires a continuum of nanoparticle contacts, with the minimum concentration ("percolation threshold") for a filler network depending on particle size, shape, and interaction with the polymer. This threshold represents the minimum particle volume fraction necessary for the formation of a space-spanning network, which can be either formed by bare clusters or mediated by a fraction of adsorbed polymer.[8] The presence of a network confers nonlinearity to the mechanical response, since the particle contacts can be broken by strain.[9]

For the commonly used nanofillers, the percentage of the nanoparticles in the nanocomposite is usually quite low because of the low nanoparticle percolation threshold. However, when the nanoparticle content increases beyond the percolation threshold, the nanocomposite can lose its beneficial properties.[4] Thus, the knowledge of the percolation threshold is important in the designing of nanocomposites.

Generally, nanocomposites can be obtained either by mixing the filler with the polymer melt or "*in situ*" by polymerization of a monomer containing dispersed filler. The latter method enables better dispersion of the filler (at the nanoscale) in comparison with the former one, because the inherently high viscosity of the polymer melt often hinders the dispersion of the additives. An especially useful polymerization method is a UV-induced process, widely used in industry,[10–12] which is solvent-free, energy efficient and can be realized at ambient temperature with high speed. Investigation of the formation of nanocomposites during the photopolymerization process is the subject of the presented work.

The clustering of nanoparticles and formation of a connected network were studied using spectroscopic methods (instead of widely used rheological or mechanical techniques). An

important issue, that have not been explored so far, was to study the effect of silica clustering on the curing kinetics for the range of silica concentrations encompassing the percolation threshold. These studies were supported by investigations of surface morphology using AFM.

A fine dispersion of silica nanoparticles in the monomer is achieved during the homogenization process, which breaks up the initial aggregates down to small clusters of primary particles. However, during the polymerization the clusters have a tendency to reassemble into bigger structures, which may span the whole space depending on filler content and interactions between the components.[8] After reaching the percolation threshold the system consists of a three-dimensional network of nanoparticle clusters interpenetrated with the polymer matrix. Such an agglomeration process influences the relaxation dynamics and the elastic properties of the system. Changes in these properties can be precisely observed using Brillouin spectroscopy. As it will be shown later, this method proved to be very useful to study the percolation threshold and viscoelastic properties of composites. A supplementary method was Raman scattering, which gives information on the degree of silica dispersion and particle mobility in the nanocomposites under study.

The polymer selected for the investigations should be highly compatible with the filler, which in turn must be thoroughly dispersed in the polymer matrix to the nanolevel. The system, which meets these requirements is poly(2-hydroxyethyl acrylate), PHEA, filled with fumed nanosilica. PHEA forms a flexible, rubbery polymer matrix, which facilitates the observation of changes in elasticity after silica addition. The nanosilica used herein (Aerosil 200) consists of spherical particles having surfaces covered with hydroxyl groups, which should provide good affinity of the filler with the monomer and polymer.

Hence, the aim of the work was to investigate the effect of clustering of nanosized silica on viscoelastic properties, curing kinetics, and morphology of the polyacrylate/nanosilica system for a wide range of silica concentrations encompassing the percolation threshold.

EXPERIMENTAL

Materials

The monomer, 2-hydroxyethyl acrylate (HEA) (purity 96%, Aldrich) was used as received. The photoinitiator, 2,2-dimethoxy-2-phenylacetophenone (Irgacure 651) and nanosilica, Aerosil 200, were kindly donated by Ciba and Evonik, respectively.

Aerosil 200 is a hydrophilic fumed silica with a specific surface of 200 $m^2\ g^{-1}$ and an average primary particle size of 12 nm.[13] The silica was dried at 110°C for 2 h before use. The monomer/filler mixtures containing different amount of silica (2–30 wt %) and the photoinitiator (0.2 wt % for kinetic measurement and 1 wt % for composite samples; photoinitiator concentration was calculated with respect to the monomer) were homogenized by ultrasonication through 2–20 h.

Methods

Photopolymerization Kinetics. Reaction rates (R_p) and conversions (p) were determined by differential scanning calorimetry (DSC) under isothermal conditions at (30 ± 0.01°C) in a high-purity argon atmosphere (<0.0005% of O_2) using the Pyris 6 instrument (Perkin-Elmer) equipped with a lid designed for photochemical measurements. The procedure was the same as described previously.[14] The 2 mg samples were polymerized in open aluminum pans with the diameter of 6.6 mm. The polymerizations were initiated by the light from a LED Hamamatsu LC-L1 lamp ($\lambda = 365$ nm, light intensity at the sample pan position 2.75 mW cm^{-2}). All DSC photopolymerization experiments were conducted at least in triplicate. The reproducibility of the results was about ±3%. For computations, the heat of polymerization was taken to be 56 kJ/mol per one double bond.

Sample Preparation for Brillouin and Raman Measurements

Samples of composites (dimensions: 10 × 15 × 2.5 mm) were obtained by the photopolymerization of the monomer/silica mixtures in a special steel mold. The samples were irradiated for 3 min from both sides through PET foils with the full spectrum of a DYMAX-Blue Wave 50 lamp.

Brillouin Scattering Measurements

The main purpose of Brillouin spectroscopy is the investigation of propagation of acoustic waves in the medium. The velocity of sound propagation depends on the elasticity of the medium. The acoustic waves undergo damping, the magnitude of which depends on elasticity of the medium, defects, relaxation processes, etc. The adiabatic compressibility β describes the susceptibility of a medium to deformation, whereas the attenuation coefficient α describes damping processes, in this case the damping of acoustic waves.[15,16] Thus, any changes in viscoelastic properties of the composite (associated with the silica loading level and interactions between the components) will influence these parameters.

A spectrometer and experimental procedure used in a Brillouin experiment were described in details elsewhere.[17] As the source of excitation light, we used argon ion laser operating at $\lambda = 514.5$ nm. The accuracy of the Brillouin shift was ± 0.1% and the full width at half the maximum $2\Gamma_B$ was ±2%.

The hypersonic velocity V was calculated as:

$$V = \frac{\Delta\omega_B \cdot c}{2n \cdot \omega_0 \cdot \sin(\Theta/2)}, \quad (1)$$

where $\Delta\omega_B$ is the Brillouin shift estimated from the Brillouin spectrum, c is the light velocity in vacuum, n is the refractive index of the scattering composition (1.450 for neat HEA at 514.5 nm; for the composition containing the highest amount of silica it did not change more than 6%), ω_0 is the frequency of the incident light (583 × 10^3 GHz) and Θ is the scattering angle (90°).

The refractive indices n for PHEA and PHEA/silica composites were estimated from Brillouin measurements performed for two different angles of scattered light: 45° and 90°. The adiabatic compressibility was calculated as:

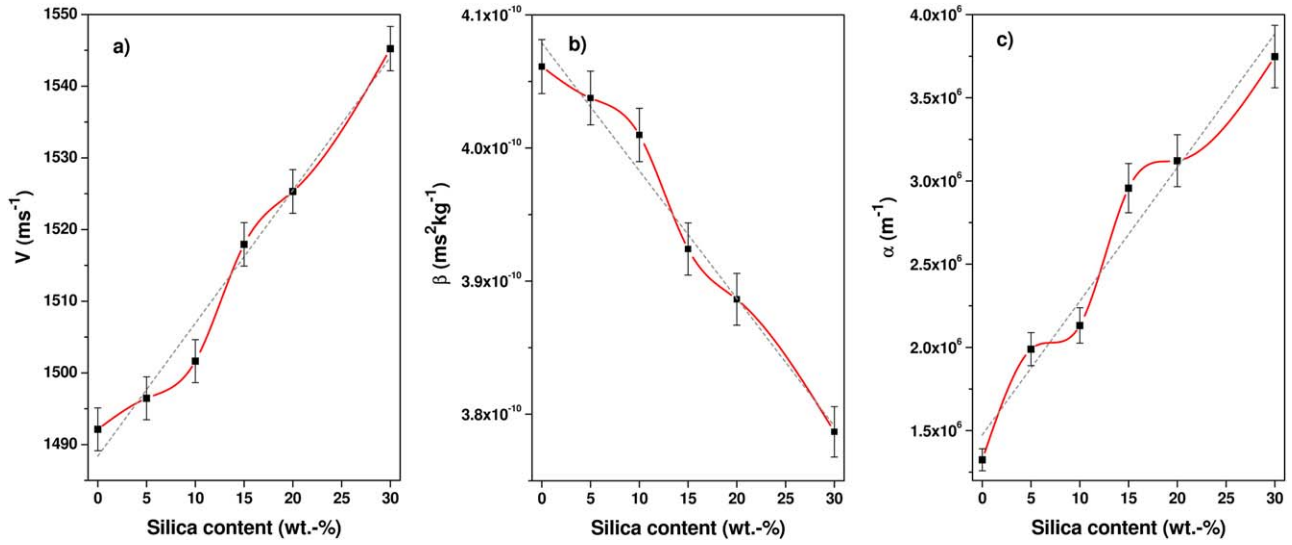

Figure 1. Hypersonic velocity V (a), adiabatic compressibility β (b), and attenuation coefficient α (c) as a function of silica content in HEA/silica mixtures. [Color figure can be viewed in the online issue, which is available at wileyonlinelibrary.com.]

$$\beta = 1/\rho V^2, \tag{2}$$

where ρ is the density of the scattering system (the value measured for the monomer was 1.011 g/cm^3 and changed by about 20% for the composition containing 30 wt % of the filler).

In calculations of the adiabatic compressibility β, we used the density estimated for the initial monomer/silica dispersions. The attenuation coefficient α was estimated as:

$$\alpha = 2\pi \cdot \Gamma_B / V \tag{3}$$

The measurements were performed for three samples of each silica content. Every sample was measured at least five times; the results were averaged and standard mean deviation was calculated.

Raman Scattering Measurements

The nonpolarized Raman spectra were recorded in back scattering geometry using Renishaw's inVia microRaman system. The measurements were performed in air at room temperature. We have used an infrared solid state laser operating at $\lambda = 785$ nm. The laser beam was tightly focused on the sample surface through the Leica 50× LWD microscope objective (LWD: long working distance). To prevent any damage of the sample the excitation power was fixed at 20 mW. The Raman spectra were recorded with a spatial resolution of about 1 μm, a spectral resolution of 1 cm^{-1}.

The measurements were performed at least three times for three samples of each silica content; the results were averaged and standard mean deviation was calculated.

AFM Measurements

AFM tapping mode was used for samples prepared by photopolymerization in DSC sample pans in the DSC instrument under Ar atmosphere. Topography and phase images were obtained in the Dimension 3100 AFM (Veeco/Bruker) controlled by the Nanoscope IIIa controller (Digital Instruments). Standard tetrahedral silicone tips (model OMCL-AC160TS, Olympus, Japan) of radius <10 nm were used. The samples were measured at room temperature.

The samples were characterized by the mean roughness R_a expressed as the average deviation of the profile from a mean line for a cross section of the sample topography. The methodology of AFM imaging and R_a calculation were the same as shown in our previous contributions.[14,18]

All samples for AFM study were tripled (separate preparation procedure). The roughness measurements were determined for the scan area of 100 μm^2, and measured at three different spots at each, individual samples' surface. This gives 9 values of R_a for one type of sample, which later were averaged, and standard mean deviation was calculated.

RESULTS AND DISCUSSION

The investigations were performed for compositions containing 2, 4, 5, 7, 10, 15, 20, and 30 wt % of silica. All monomer/silica mixtures were transparent, showing a very good dispersion of the filler.

Particle Clustering

Brillouin Scattering. Physical parameters characterizing the viscoelastic properties of the medium, that is, hypersonic velocity V, attenuation coefficient α, and adiabatic compressibility β as a function of the filler content for both the HEA/silica mixtures (before the polymerization) as well as for the PHEA/silica composites (after the polymerization) are presented in Figures 1 and 2.

In the unfilled medium, the acoustic waves propagate through the liquid monomer or the solid polymer. When an additional phase is introduced, this mechanism can be disturbed. The presented plots clearly show that all measured physical parameters are very sensitive to the silica content both in the system before the polymerization as well as in the resulting composite.

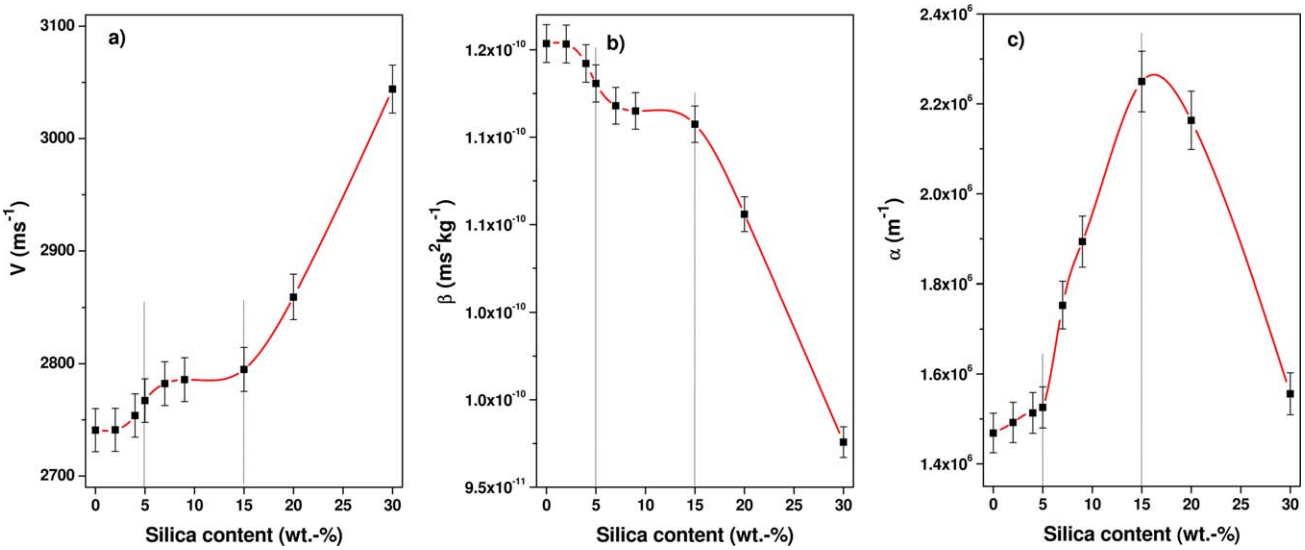

Figure 2. Hypersonic velocity V (a), adiabatic compressibility β (b), and attenuation coefficient α (c) as a function of silica content in PHEA/silica composites. [Color figure can be viewed in the online issue, which is available at wileyonlinelibrary.com.]

Before polymerization (monomer/silica dispersions, Figure 1) the measured parameters V and α increase monotonically with the increase in silica content, whereas β decreases. All presented dependences V, β, $\alpha = f$ (silica content) are practically linear with some scatter of experimental points. Introducing the silica to the monomer should increase the macroscopic elasticity of the system if good compatibility between the components exists. Thus, the higher the silica content, the more elastic the material should be. In our system, this feature is manifested by the increase in the hypersonic velocity and the decrease of the adiabatic compressibility (the adiabatic compressibility describes the susceptibility of the medium to deformation, because β is inversely proportional to the squared sound velocity). However, the attenuation coefficient α, which describes the nonelastic (viscous) response of the material, increases with the silica loading despite the rise of the macroscopic elasticity of the medium. This in turn can be explained by the interaction of the silica with the monomer molecules. The silica particles absorb the energy and dissipate it, causing a strong damping enhancement. The higher the silica content, the stronger the energy dissipation before polymerization in the unordered liquid medium consisting of small and mobile molecules.

After polymerization (polymer/silica composites, Figure 2) the medium is a solid consisting of long polymer chains of reduced mobility. This mobility is additionally restricted by the presence of silica nanoparticles. Transformation of the propagating medium from a liquid to a solid results in a significant increase in the speed of propagation of the acoustic waves as compared to the values prior to polymerization. Generally, the character of the dependence of V and β on the filler content is similar to that before the polymerization – V increases and β decreases. The main difference is that these dependences are no longer linear. Considerable behavior shows the attenuation coefficient, which will be discussed below.

The observed changes in the values of the parameters discussed reflect changes in viscoelastic properties of the polymer/silica composites at different loading levels. Therefore, the curves in Figure 2 can be divided into three stages, which correspond to different clustering regimes.[19]

In the prepercolation regime, for silica content up to about 5%, there is a slight increase in the speed of sound with increasing filler content, accompanied by a decrease of the compressibility β. This can be interpreted as an increase in the elasticity of the material, resulting from dispersion of silica particles in the polymer matrix. Silica particles also cause a damping of acoustic waves, which is manifested by a slight increase in the α values.

The percolation regime occurs for the silica content in the range of about 5–15 wt %. In this regime, the percolating paths are formed and all three dependences change their slope. The increase in the V values and the decrease of β values with the increase of the filler content are stronger to some extent than in the prepercolation regime, pointing to a further increase in the elasticity of the material. A strong and rapid rise is observed in the case of the attenuation coefficient α. The results indicate that such an interaction causes dissipation of energy, which in consequence leads to a strong intensification of damping.

When the amount of silica in the composite exceeds 15 wt %, the postpercolation regime begins. In this regime silica aggregates are directly connected and form a continuous network. The values of V and β change dramatically, indicating a strong elasticity enhancement. However, the α parameter shows a different behavior, reaching the maximum at 15 wt % of silica loading and rapidly decreasing at the higher filler content. In this case, the continuity of the network connections enables energy transfer directly between silica particles, without the mediation of the polymer chains. So, most of the energy is not dissipated, but transmitted by the filler, which causes the reduction of damping. Apparently, ~15 wt % is the critical loading corresponding to the percolation threshold.

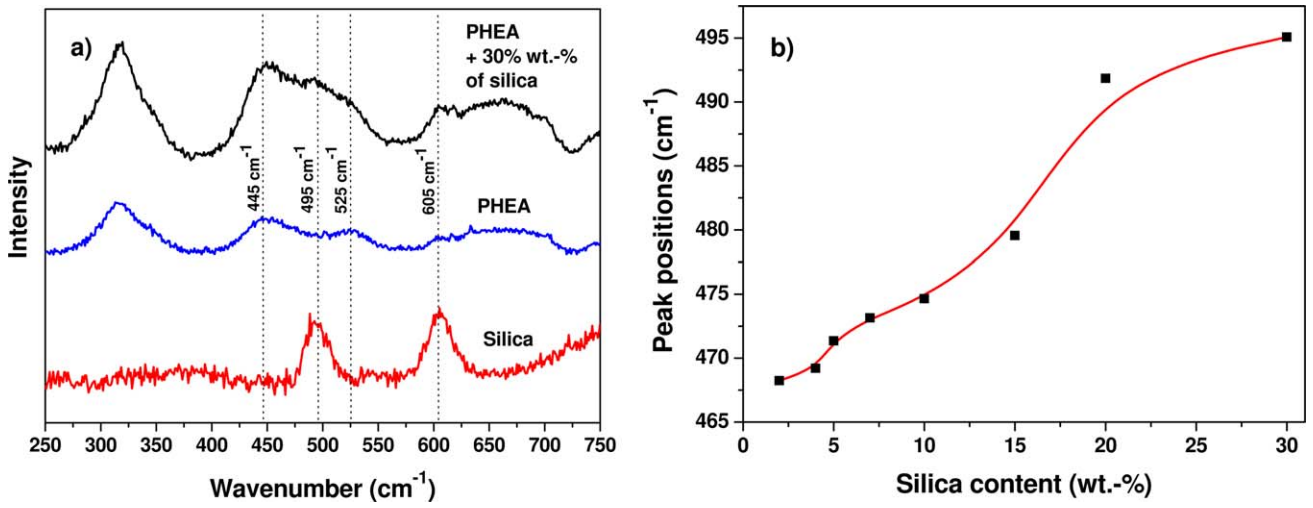

Figure 3. Raman spectra of silica, PHEA, and the nanocomposite filled with 30 wt % of silica (a) and position of D1 band in PHEA/silica composite as a function of silica content (b). [Color figure can be viewed in the online issue, which is available at wileyonlinelibrary.com.]

It is interesting that the percolation threshold of about of 15% of silica content was also suggested earlier on the basis of other experimental techniques for PHEA/silica nanocomposites, using the silica prepared in a sol-gel process.[20–22] This indicates the similarity in properties of composites described in the cited articles and obtained in our work, despite significant differences in the properties of the two silicas.

Raman Scattering

Before polymerization, the Raman spectra of the neat monomer and dispersions containing up to 30 wt % of silica do not show any differences. This means that no bands ascribed to the silica appear and it also suggests that the intensity of silica absorption is negligibly small compared with the monomer absorption. The observed phenomenon is probably associated with the size and mobility of silica particles. When the filler is well dispersed in the monomer (very small aggregates), its particles possess great freedom of movement in the liquid medium composed of small molecules. In consequence, they do not participate in energy scattering.

In contrast to the monomer/silica dispersion, bands derived from the silica can be observed in the spectra of the polymerized samples. Silica clusters embedded in the solid polymer matrix are immobile enough to scatter the energy, which results in the appearance of silica bands in the spectral range of 400–650 cm^{-1} [Figure 3(a)]. Two bands, positioned at about 495 and 605 cm^{-1}, can be attributed to deformation bands D1 (O_3SiOH tetrahedral vibration) and D2 [$(SiO)_3$ ring breathing vibrations], respectively.[23,24] Due to their very low intensity, these bands become noticeable in the spectra of the composites only at the highest silica loadings [as for 30 wt % of silica, Figure 3(a)].

The integral intensity of the D1 band increases with the silica content, because the D1 band is associated with the external layer of silica particles.[23,24] Unfortunately, the bands derived from the polymer matrix and those from the silica overlap strongly. The deconvolution[25] of band at 495 cm^{-1} (D1) derived from the silica and bands at 445 and 525 cm^{-1} associated with the polymer matrix enables to observe that the position of the D1 band shifts to higher frequencies with the increasing silica content [Figure 3(b)]. Moreover, the position of the silica band in the spectrum of the composite containing 30 wt % of the filler is close to that in the spectrum of neat silica. Thus, we can also interpret the obtained result as the shift of the Raman band of the neat silica to lower frequencies due to "dilution" by the polymer matrix. Generally, the vibration energy is determined by the vibrations of the individual particles. In the neat silica, the motion of the particles is strongly restricted and the vibration energy is the highest. As the particles become diluted by the polymer phase they gain some freedom and lose a part of their energy. The smaller and more diluted the aggregates, the higher the energy loss. This results in the observed shift of the Raman band position to lower frequencies. However, the dependence of the peak position on the filler content is not linear. Above ~15–20 wt % of the silica there is a slight decrease in the slope. This can be associated with a "saturation effect" being a consequence of the formation of the three-dimensional network of nanoparticle clusters interdispersed with the host polymer (percolation threshold). In the continuous phase, silica particles are so densely packed that further increase of their content cannot affect the vibrational energy to a significant degree. At 30 wt % of the filler the D1 band position reaches a value close to that obtained for the neat silica.

Photopolymerization Kinetics

As the structure of the composite is formed during the curing process, it can be expected that the formation of the continuous silica phase, which must occur during early stages of the polymerization, will influence the kinetics of the curing process.

The photopolymerization kinetics was studied at 30°C. The dependence of the polymerization rate R_p on the irradiation time t for formulations with different silica contents is depicted in Figure 4(a). The curves show an immediate onset of autoacceleration and occurrence of a maximum polymerization

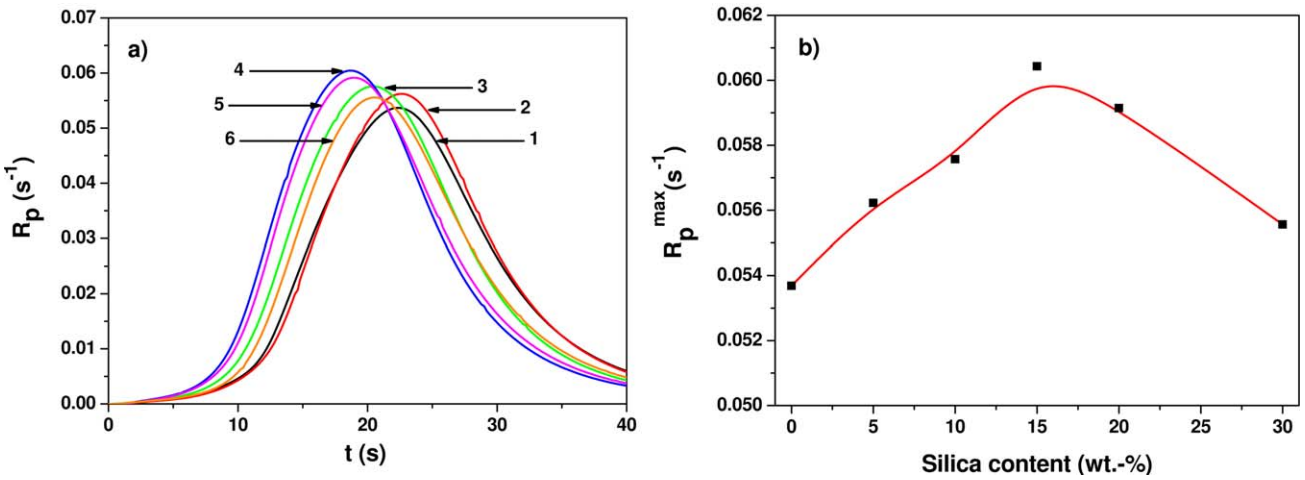

Figure 4. Polymerization rate R_p of HEMA as a function of irradiation time t at 30°C for different silica contents; the numbers 1–6 correspond to silica content 0, 5, 10, 15, 20, and 30 wt %, respectively (a), and maximum polymerization rate R_p^{max} as a function of silica content (b). [Color figure can be viewed in the online issue, which is available at wileyonlinelibrary.com.]

rate R_p^{max}. These phenomena are typical for the polymerization of acrylates. The addition of the silica to the monomer affects the kinetics of the polymerization process and generally we observe an enhancement of the gel effect (a reduction of the induction period, an increase in R_p and R_p^{max}). However, the changes in R_p and R_p^{max} are not monotonic. After reaching the maximum value for the composition containing 15 wt % of the silica, R_p^{max} [Figure 4(a,b)] starts decreasing with an increase in silica content and the reaction slows down. A similar effect was observed for other matrices: in[14] for 5%, in[26] for 10% and in[27] for 15% of silica content. The suggested explanations were based on scattering of light by the silica[26,27]; none of them was associated with the percolation threshold.

The final conversion degree p^f is high (the highest value obtained is 0.86) and show a similar trend as R_p^{max}. However, in this case the influence of the silica is very small and p^f changes in the range of only 0.03. This is because composites remain flexible, above the glass transition temperature T_g, in the whole range of the silica content providing high mobility to the system (which in turn determines the final degree of conversion). T_g of the composites increases from 13.9°C for the neat PHEA to 15.3°C for the composite containing 30 wt % of the silica. The continuous increase of T_g indicates the interaction between PHEA and the silica.

The increase in the polymerization rate is often associated with the increase in viscosity of the system, which suppresses the termination by slowing the diffusion of macroradicals and thereby accelerates the polymerization.[14] Because the termination rate coefficient k_t^b is inversely proportional to the viscosity ($k_t^b = 1/\eta$) and the polymerization rate R_p is related to the termination rate coefficient as $R_p = 1/(k_t^b)^{0.5}$, the increase in the initial viscosity of the formulation should result in a faster polymerization. The macroscopic viscosity of the initial monomer/silica dispersions increases monotonically with the filler content from 4 mPa·s for the unfilled monomer up to 118 mPa·s at the 30 wt % silica loading (measured at the polymerization temperature 30°C). However, the viscosity of the monomer/silica mixture is determined by the interaction between the silica particles and the monomer, although the viscosity of the bulk monomer on the molecular level will be less affected than the overall viscosity. During polymerization, attractive interactions between the silica surface and polymer chains additionally alter the mobility of the polymer segments through the creation of the interphase region. In this region polymer mobility changes in a gradient fashion away from the polymer-surface interface.[19] This also applies to growing macroradicals, and their immobilization on silica particles along with increased initial viscosity seem to be the main reasons for suppressed termination and enhanced polymerization rates for compositions containing up to 15 wt % of the silica.

However, the decrease of the R_p^{max} value is often associated with the high initial viscosity of the system, which leads to early diffusional control of propagation.[28,29] Nevertheless, the initial viscosities of the HEA/silica mixtures are too low to cause such a phenomenon. Generally, the most reactive composition (showing the highest R_p^{max} value) can be expected when the interactions between the monomer and the filler are the strongest and the system is the most stable, as it was suggested in our previous article.[14] When the silica content exceeds 15 wt %, the self-attraction between nanoparticles dominates and leads to extensive clustering. Diffusivity of monomer molecules decreases, which deteriorates the propagation conditions and leads to the observed decrease of both the polymerization rate R_p and the maximum polymerization rate R_p^{max}. Since gelation starts from the beginning of the reaction, the silica particles are immobilized in the polymer matrix from the early stages of the polymerization and in the consequence, the kinetics is affected also from the beginning of the reaction.

AFM

AFM experiments were performed for PHEA and composites containing 5, 10, 15, 20, and 30 wt % of the silica. Figure 5 presents AFM images of the phase (left column), height (topography, middle column), as well as the section analysis plots (right column) for the neat PHEA and the composites

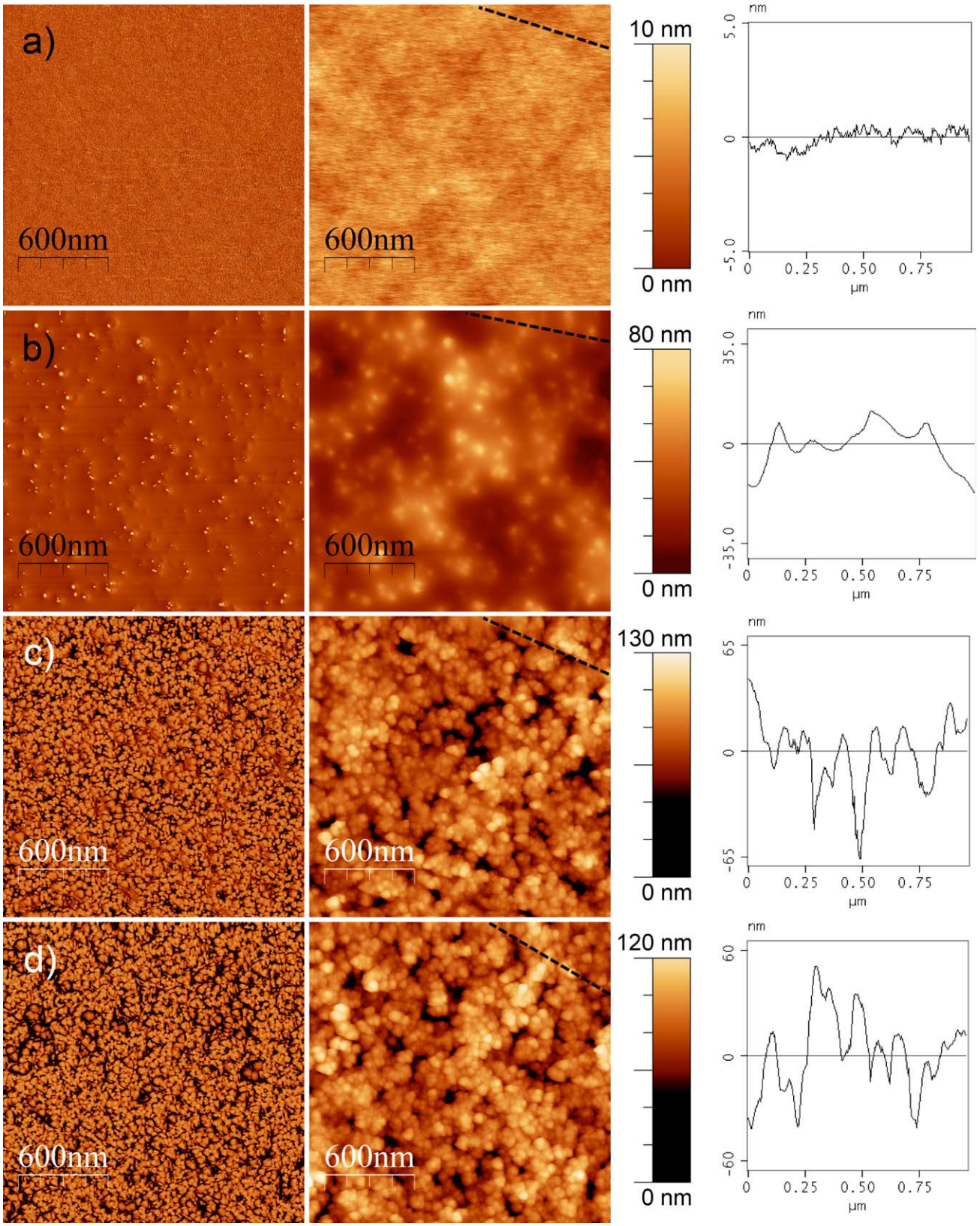

Figure 5. AFM images of PHEA (a), and PHEA filled with 5 wt % (b), 10 wt % (c), and 20 wt % (d) of silica. First and second column represents phase and height images, respectively. Black dashed lines represent the profile of section analysis. Section analysis plots are shown on right. [Color figure can be viewed in the online issue, which is available at wileyonlinelibrary.com.]

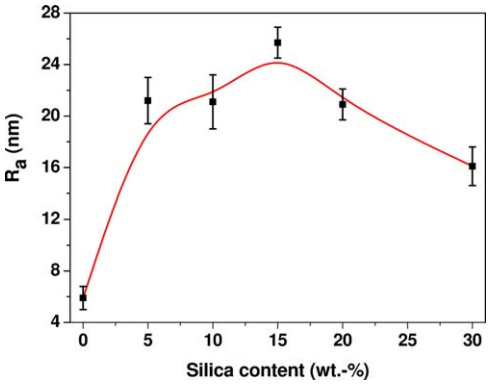

Figure 6. Mean roughness R_a as function of silica content. The error bars indicate the standard deviation of mean value. [Color figure can be viewed in the online issue, which is available at wileyonlinelibrary.com.]

containing 5, 10, and 20 wt % of the silica. The surface of the neat PHEA is completely flat and homogenous without any cracks and voids as it can be seen in the height image and section analysis plot in Figure 5(a). The phase image shows no difference in mechanical compliance of the sample surface (no difference in brightness in the phase image), which confirms its homogeneity. At the low filler loading (5 wt %) single and aggregated silica particles are exposed on the surface. They can be seen as convex-features (bright spots) in the height image in Figure 5(b). The planar-size of the discussed structure is shown in the section analysis plot [Figure 5(b)].

The increase in the silica content to 10 wt % and higher changes the surface structure [compare Figure 5(b) vs. 5(c,d)]. The silica particles densely cover the surface creating an aggregate-to-aggregate system as it can be seen in the height, phase image, and section analysis plot. The aggregates are well and uniformly dispersed at the interface. The planar-size of aggregates ranges from 20 to 70 nm. This corresponds to ~1–5 single silica nanoparticles in one aggregate (the particles are covered by several nm thick polymer layers[30]). However, this is only a rough estimation.

The differences in the topography of the investigated composites, especially at high silica loadings, can be quantified by comparing the R_a values (Figure 6). The addition of only 5 wt % of the silica leads to a rapid increase in the R_a value (21.2 nm), which is approx. four times higher in comparison to the neat PHEA (5.9 nm). R_a increases with the silica content and reaches the maximum at 15 wt % filling, that is, at the percolation threshold. Further increase in the silica content leads to the reduction of the R_a value. This can be taken as an indication that the size of aggregates decreases when the silica content exceeds 15 wt %, that is, the silica clusters and the interphase become more uniformly dispersed in the polymer matrix. It is associated with a larger number of clusters formed at the higher filler content and a partial destruction of the interphase network beyond the percolation threshold.[19] A similar tendency in R_a has been recently observed by us for a crosslinked polymer/nanosilica system.[14]

AFM results are in good agreement with the kinetic, Brillouin and Raman spectroscopy results. They suggest substantial changes in the morphology of the composite when the silica content exceeds the threshold level.

CONCLUSIONS

The formation of the cocontinuous silica phase significantly affects damping of acoustic waves (as observed by Brillouin spectroscopy) in polymer/silica nanocomposites due to the change in the mechanism of energy transfer. Differences between the energy loss through small silica clusters dispersed in the polymer matrix and those densely packed in the percolating network are also reflected in the Raman spectra.

The increase of the polymerization rate of the monomer with increasing silica content up to the percolation threshold is a consequence of the immobilization of growing macroradicals on silica particles and increased initial viscosity, which cause suppression of the termination reaction. However, the reduction of the monomer diffusivity resulting from extensive silica clustering above the percolation threshold restricts the propagation conditions and is responsible for slowing down the polymerization.

The surface morphology depends on the degree of clustering of silica particles. The surface roughness reaches maximum at the percolation threshold, which can be associated with a partial destruction of the interphase network due to the formation of larger number of clusters.

ACKNOWLEDGMENTS

This work was supported by the Research Projects of Poznan University of Technology 64-001/12 DS-PB and 32-173/2012 DS-PB and research project N N209 339437. HG acknowledges the Polish Ministry of Science and Higher Education for the project "Mobilność Plus" No. 650/MOB/2011/0 and financial supports from the project "Scholarship support for Ph.D. students specializing in major strategies for Wielkopolska development", Sub-measure 8.2.2 Human Capital Operational Programme, co-financed by European Union under the European Social Fund.

REFERENCES

1. Paul, D. R.; Robeson, L. M. *Polymer* **2008**, *49*, 3187.
2. Jordan, J.; Jacob, K. I.; Tannenbaum, R.; Sharaf, M. A.; Jasiuk, I. *Mater. Sci. Eng. A* **2005**, *393*, 1.
3. Jouault, N.; Vallat, P.; Dalmas, F.; Said, S.; Jestin, J.; Boue, F. *Macromolecules* **2009**, *42*, 2031.
4. Danikas, M. G.; Tanaka, T. *IEEE Electr. Insul. Mag.* **2009**, *25*, 19.
5. Sun, L. L.; Zhao, Y.; Zhong, W. H. *Macromol. Mater. Eng.* **2011**, *296*, 992.
6. Nogales, A.; Broza, G.; Roslaniec, Z.; Schulte, K.; Sics, I.; Hsiao, B. S.; Sanz, A.; Garcia-Gutierrez, M. C.; Rueda, D. R.; Domingo, C.; Ezquerra, T. A. *Macromolecules* **2004**, *37*, 7669.
7. Ramanathan, T.; Stankovich, S.; Dikin, D. A.; Liu, H.; Shen, H.; Nguyen, S. T.; Brinson, L. C. *J. Polym. Sci. Part B: Polym. Phys.* **2007**, *45*, 2097.

8. Filippone, G.; Salzano De Luna, M. *Macromolecules* **2012**, *45*, 8853.
9. Bogoslovov, R. B.; Roland, C. M.; Ellis, A. R.; Randall, A. M.; Robertson, C. G. *Macromolecules* **2008**, *41*, 1289.
10. Oh, S. J.; Lee, S. C.; Park, S. Y. *Vib. Spectrosc.* **2006**, *42*, 273.
11. Andrzejewska, E. *Prog. Polym. Sci. (Oxford)* **2001**, *26*, 605.
12. Seo, J.; Jang, E. S.; Song, J. H.; Choi, S., Khan, S. B.; Han, H. *J. Appl. Polym. Sci.* **2010**, *118*, 2454.
13. Evonik Degussa (Technical Information), **2006**.
14. Sadej-Bajerlain, M.; Gojzewski, H.; Andrzejewska, E. *Polymer* **2011**, *52*, 1495.
15. Arecchi, F. T.; Schultz-Dubois, E. O. Laser Handbook; North-Holland Pub. Co., Amsterdam, **1972**.
16. Brillouin, L. *Ann. de Phys.* **1922**, *17*, 88.
17. Ziobrowski, P.; Nowicka, A.; Andrzejewska, E.; Marcinkowska, A.; Drozdowski, M. *Spectrochim. Acta Part A* **2011**, *79*, 815.
18. Richter, A.; Gojzewski, H.; Belbruno, J. *J. Int. J. Mater. Res.* **2007**, *98*, 414.
19. Qiao, R.; Deng, H.; Putz, K. W.; Brinson, L. C. *J. Polym. Sci. Part B: Polym. Phys.* **2011**, *49*, 740.
20. Hernandez, J. C. R.; Pradas, M. M.; Ribelles, J. L. G. *J. Non-Cryst. Solids* **2008**, *354*, 1900.
21. Hernandez, J. C. R.; Sanchez, S. M.; Gomez Ribelles, J. L. G.; Pradas, M. M. *Eur. Polym. J.* **2007**, *43*, 2775.
22. Pandis, C.; Spanoudaki, A.; Kyritsis, A.; Pissis, P.; Hernandez, J. C. R.; Gomez Ribelles, J. L.; Monleon Pradas, M. *J. Polym. Sci. Part B: Polym. Phys.* **2011**, *49*, 657.
23. Ivanda, M.; Clasen, R.; Hornfeck, M.; Kiefer, W. *J. Non-Cryst. Solids* **2003**, *322*, 46.
24. Phillips, J. C. *Solid State Phys. Adv. Res. Appl.* **1983**, *37*, 93.
25. Lin, W.; Cossar, M.; Dang, V.; Teh, J. *Polym. Test.* **2007**, *26*, 814.
26. Li, F.; Zhou, S.; You, B.; Wu, L. *J. Appl. Polym. Sci.* **2006**, *99*, 1429.
27. Cho, J. D.; Ju, H. T.; Hong, J. W. *J. Polym. Sci. Part A: Polym. Chem.* **2005**, *43*, 658.
28. Marcinkowska, A.; Andrzejewska, E. *J. Appl. Polym. Sci.* **2010**, *116*, 280.
29. Andrzejewska, E.; Marcinkowska, A. *J. Appl. Polym. Sci.* **2008**, *110*, 2780.
30. Camenzind, A.; Caseri, W. R.; Pratsinis, S. E. *Nano Today* **2010**, *5*, 48.